RSC Advances

PAPER

View Article Online
View Journal | View Issue

Cite this: *RSC Adv.*, 2026, **16**, 4204

Coexistence of ferroelectricity and altermagnetism in wurtzite vanadium oxide: a first-principles study

Abid Zaman, *[a] Salhah Hamed Alrefaee,[b] Hifsa Shahid,[c] Tatyana Orlova,[d] Aeshah Alrubayyi,[e] Reem Alreshidi,*[f] Vineet Tirth[gh] and Ali Algahtani[gi]

Multiferroic and altermagnetic materials that simultaneously exhibit coupled electric and magnetic functionalities have emerged as promising candidates for next-generation spintronic and memory devices. In this work, we present a comprehensive first-principles investigation of bulk wurtzite vanadium oxide (w-VO), revealing its unique coexistence of robust ferroelectricity and altermagnetism. The w-VO compound crystallizes in a non-centrosymmetric hexagonal wurtzite phase (space group $P6_3mc$), confirmed to be both thermodynamically and dynamically stable. Magnetic energy analysis identifies a layered antiferromagnetic (AFM) ground state with a local V magnetic moment of 2.42 μB, yielding a fully compensated magnetization. The electronic structure displays momentum-dependent spin splitting of ~50 meV in the valence band along non-symmetric k-paths, a defining characteristic of altermagnetism arising from crystal symmetry and magnetic ordering rather than spin–orbit coupling. Furthermore, the system exhibits an in-plane magnetic easy axis and a substantial spin Hall conductivity (SHC), peaking at −182 ($\hbar/e$) S cm^{-1} under hole doping, surpassing values reported for known spin Hall materials. Remarkably, w-VO also demonstrates a strong out-of-plane spontaneous polarization of 113.12 μC cm^{-2} along the [001] direction, substantially higher than conventional perovskite ferroelectrics. The polarization switching process, with a moderate energy barrier of 0.71 eV per f.u., confirms its ferroelectric reversibility. Strikingly, reversing the ferroelectric polarization induces a complete reversal of spin character near the Fermi level, thereby electrically toggling the spin-resolved electronic structure without altering the total magnetization. These findings establish w-VO as a rare multiferroic altermagnet in which ferroelectric polarization and compensated spin order are intrinsically coupled. The ability to control spin polarization and spin Hall response through electric-field-driven polarization switching offers a new paradigm for non-volatile, field-free spintronic devices based on voltage-controlled spin functionality.

Received 19th November 2025
Accepted 7th January 2026

DOI: 10.1039/d5ra08930a

rsc.li/rsc-advances

Introduction

In recent years, altermagnetism has emerged as a distinct magnetic phase characterized by compensated magnetic order coexisting with momentum-dependent spin polarization enforced by crystal symmetry. Unlike conventional antiferromagnets, altermagnets exhibit non-relativistic spin splitting in their electronic band structures, even in the absence of net magnetization and spin–orbit coupling, arising from the interplay between magnetic ordering and non-primitive symmetry operations of the lattice.[1–3] This intrinsic spin polarization enables the generation and manipulation of spin-polarized electronic states without external magnetic fields, offering new opportunities for energy-efficient spintronic applications.[4,5] Several representative altermagnetic materials, including MnTe, RuO_2, and Mn_5Si_3, have been shown to exhibit pronounced transport phenomena such as the anomalous Hall effect, originating from Berry curvature generated by their unique momentum-space spin texture.[2,6,7] These findings highlight

[a]*Department of Physics, Riphah International University, Islamabad 44000, Pakistan. E-mail: zaman.abid87@gmail.com*
[b]*Department of Chemistry, College of Science, Taibah University, Yanbu Governorate, Saudi Arabia*
[c]*Department of Electrical Engineering, College of Engineering, Qassim University, Unayzah, Saudi Arabia*
[d]*Department of Physics and its Teaching Methods, National Pedagogical University of Uzbekistan, Tashkent, Uzbekistan*
[e]*Department of Science and Technology, University College at Nairiyah, University of Hafr Al Batin (UHB), Nairiyah, 31981, Saudi Arabia*
[f]*Department of Physics, College of Science, Northern Border University, Arar, Saudi Arabia. E-mail: Reem.Alreshidi@nbu.edu.sa*
[g]*Mechanical Engineering Department, College of Engineering, King Khalid University, Abha 61421, Aseer, Kingdom of Saudi Arabia*
[h]*Centre for Engineering and Technology Innovations, King Khalid University, Abha 61421, Aseer, Kingdom of Saudi Arabia*
[i]*Research Center for Advanced Materials Science (RCAMS), King Khalid University, Guraiger, P.O. Box 9004, Abha-61413, Aseer, Kingdom of Saudi Arabia*

the broader significance of altermagnetism for Berry-phase-driven transport and motivate the search for new altermagnetic platforms with additional functional degrees of freedom.[8]

Parallel to the progress in altermagnetic research, transition metal oxides (TMOs) have remained central to condensed matter and materials science due to their wide-ranging structural versatility and multifunctional physical responses. Many TMOs crystallize in the cubic rock-salt phase, although hexagonal variants, such as those adopting the wurtzite structure, have also been experimentally realized.[9,10] A decade ago, Nam and co-workers successfully synthesized wurtzite-type MnO, an achievement that sparked[11] new interest in non-centrosymmetric oxide lattices and their potential multifunctionalities.[12] The polar wurtzite lattice, consisting of tetrahedrally coordinated atoms linked by strong covalent bonds, was historically assumed to lack switchable electric polarization. Despite its noncentrosymmetric space group ($P6_3mc$), it was widely believed that the rigid tetrahedral framework prevented ferroelectric switching. Nevertheless, a sequence of experimental and theoretical milestones gradually overturned this assumption. The earliest evidence dates back to Sawada *et al.* (1973), who reported a measurable spontaneous polarization of approximately 6.1 μC cm^{-2} at 1078 K in wurtzite BeO.[13] Two decades later, Onodera and collaborators detected a dielectric anomaly near 330 K and a weak polarization of about 0.044 C.c^{-2} in Li-doped ZnO, which was subsequently reaffirmed by Joseph *et al.* (1999) in the same compound.[14,15]

Complementary theoretical investigations were later carried out by Gopal *et al.* (2004) and Vanderbilt *et al.* (2007), who examined the piezoelectric and polarization properties of MnO and ZnO in their wurtzite configurations.[15,16] At that stage, however, the existence of spontaneous ferroelectricity in these oxides had not been suggested. The scenario evolved with the work of Moriwake *et al.* (2014), who theoretically demonstrated the feasibility of ferroelectric switching in simple chalcogenides possessing the wurtzite lattice.[17–19] Their findings encouraged several research groups to experimentally validate the ferroelectric character of wurtzite-structured compounds.[20] A decisive experimental advance arrived in 2019, when Fichtner and co-workers revealed a well-defined polarization, electric field hysteresis loop in Sc-doped AlN thin films, showing a spontaneous polarization of nearly 8.1 μC cm^{-2}.[21,22] This observation conclusively confirmed the existence of robust ferroelectricity within wurtzite-type materials and marked a significant step toward integrating them into piezoelectric and ferroelectric nano-electronic devices.[23–25] Together, these advances have reshaped our understanding of wurtzite structures by revealing an intrinsic coupling between symmetry, magnetism, and polarization. Motivated by these developments, we investigate the multifunctional properties of wurtzite vanadium oxide (VO), demonstrating that this material exhibits coexisting altermagnetic and ferroelectric behavior. Our results highlight w-VO as a promising platform for next-generation ferroelectric and spintronic technologies.

Computational techniques

The structural, magnetic, and ferroelectric characteristics of wurtzite-type VO were examined through first-principles calculations based on density functional theory (DFT), as implemented in the Vienna *Ab initio* Simulation Package (VASP).[26] The interaction between valence and core electrons was modeled using the projector-augmented wave (PAW) formalism, while the exchange–correlation energy was treated within the generalized gradient approximation (GGA) following the Perdew–Burke–Ernzerhof (PBE) functional.[27] To correctly capture the localized behavior of the V-3d orbitals, a Hubbard on-site correction (DFT+U) was employed with an effective U value of 4.0 eV, which was adopted from previous first-principles studies on vanadium-based oxides and has been widely used to describe the electronic and magnetic properties of V-3d states.[28–31] All atomic positions and lattice constants were optimized without symmetry restrictions until the energy convergence reached 10^{-6} eV and atomic forces were below 0.01 eV Å^{-1}. A plane-wave cutoff energy of 500 eV and a Monkhorst–Pack k-point grid of 15 × 15 × 13 were adopted for total energy and electronic structure evaluations.

The magnetocrystalline anisotropy energy (MAE) was computed within the non-collinear spin formalism, including spin–orbit coupling (SOC),[32] by aligning the magnetic moments along the [001], [100], [010], and [111] directions. To confirm lattice dynamical stability, the phonon dispersion was obtained using the Phonopy package with a 2 × 2 × 2 supercell and a 5 × 5 × 3 k-mesh.[33] The spontaneous polarization of w-VO was calculated within the modern theory of polarization using the Berry-phase formalism as developed by King-Smith and Vanderbilt.[34] In this framework, the total polarization (P) is expressed as the sum of the ionic contribution (P_{ion}) and the electronic component (P_{ele}) derived from the phase of occupied Bloch states across the Brillouin zone. The variation of polarization along an adiabatic path connecting the centrosymmetric (non-polar) and polar configurations (defined by a scaling parameter λ) yields the spontaneous polarization difference ΔP. To assess the energy barrier for polarization switching, the climbing-image nudged elastic band (CI-NEB) method was applied, identifying the minimum energy path (MEP) associated with V-ion displacement between two equivalent ferroelectric orientations.[35]

Results and discussion

The optimized crystal geometry of bulk wurtzite vanadium oxide (w-VO) is illustrated in Fig. 1(a) and (b), showing both top and side views of the structure. The conventional unit cell of w-VO contains two formula units (f.u.) of VO, in which each V atom is tetrahedrally coordinated by four nonmagnetic O atoms located at the vertices of the surrounding polyhedra. The system crystallizes in a non-centrosymmetric hexagonal wurtzite lattice belonging to the $P6_3mc$ (no. 186) space group. After full structural relaxation, the equilibrium lattice parameters are obtained as $a = b = 3.16$ Å and $c = 5.97$ Å. The optimized wurtzite VO polymorph exhibits a strongly non-ideal lattice ratio, $c/a \approx$

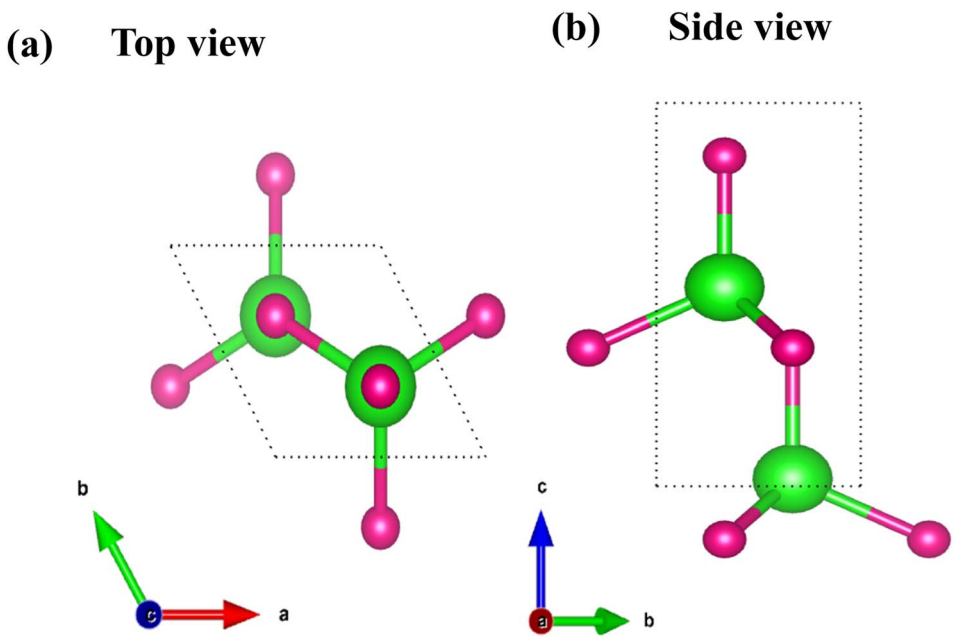

Fig. 1 Atomic structure of bulk wurtzite VO in its optimized ground state. (a) Top view along the *c*-axis, showing the in-plane arrangement of VO_4 tetrahedra within the hexagonal lattice (b) side view along the *a*-axis, illustrating the stacking of tetrahedra along the polar *c*-axis. Green and pink spheres represent V and O atoms, respectively.

1.89c, which is significantly larger than the ideal wurtzite value (~1.633) characteristic of tetrahedrally coordinated sp^3-bonded compounds such as ZnO. This pronounced deviation is physically expected because VO intrinsically favors octahedral coordination of the V–O network, as realized in the rock-salt ground state. When VO is constrained into a tetrahedrally coordinated wurtzite topology, the lattice undergoes a strong anisotropic relaxation to reduce the unfavorable crystal-field and bonding environment of the V-3d electrons. This relaxation primarily manifests as an elongation along the *c* axis, accompanied by distortions of the local V–O bond lengths and bond angles as well as a shift in the internal structural parameter *u*. Consequently, the large *c*/*a* ratio should be interpreted as a hallmark of a metastable, constraint-stabilized wurtzite-like configuration, rather than a conventional ideal wurtzite lattice. We further explored the magnetic ground state of bulk wurtzite VO (w-VO). To determine the most energetically favorable spin configuration, four different magnetic arrangements were examined within a $2 \times 2 \times 1$ supercell, including one ferromagnetic (FM) and three distinct antiferromagnetic (AFM) configurations, as illustrated in Fig. 2(a)–(d). Among these, the layered antiferromagnetic (AFM) arrangement, shown in Fig. 2(a), emerged as the lowest-energy configuration. The calculated exchange energy difference ($E_{ex} = E_{AFM} - E_{FM}$) between the most stable AFM state and the FM state is 80 meV per unit cell, indicating that the AFM alignment is strongly favored. In this ground-state configuration, each V atom carries a magnetic moment of 2.42 μB, and the antiparallel coupling between neighboring V atoms leads to an overall zero net magnetization, consistent with compensated magnetic ordering. The calculated local magnetic moment of 2.42 μB on the V atom is smaller than the spin-only effective moment (~3.9 μB) expected for an isolated, fully localized d^3 ion in the paramagnetic regime. This difference arises because the DFT value represents the ground-state local spin moment obtained by integrating the spin density within the V atomic region, rather than the Curie–Weiss effective moment. In wurtzite VO, the strong electronegativity of oxygen leads to significant charge transfer from V to O and pronounced V–O covalency, resulting in partial delocalization of the V-3d spin density onto neighboring O atoms and the interstitial region. In addition, the partial itinerant character of the V-3d states further reduces the on-site magnetic moment compared with the ideal ionic limit.

To evaluate its thermodynamic stability, the formation energy (E_F) was computed according to

$$E_F = (E_T - 2E_V - 2E_O)/N$$

where E_T is the total energy of the optimized structure, E_V and E_O represent the chemical potentials of an isolated V and O atom, respectively, and *N* denotes the total number of atoms in the simulation cell. The chemical potential of V was obtained from the body-centered cubic (bcc) V bulk phase, while that of oxygen was derived from an O_2 molecule. The calculated formation energy of −2.21 eV per atom indicates that w-VO is chemically stable with respect to elemental decomposition. Although the wurtzite phase of VO is chemically stable, it is energetically higher than the rock-salt ground state by approximately 0.8 eV per formula unit. Such an energy separation does not preclude experimental realization of the metastable phase under non-equilibrium conditions. Comparable or even larger polymorph energy differences are well documented in materials where multiple phases have been experimentally fabricated. A

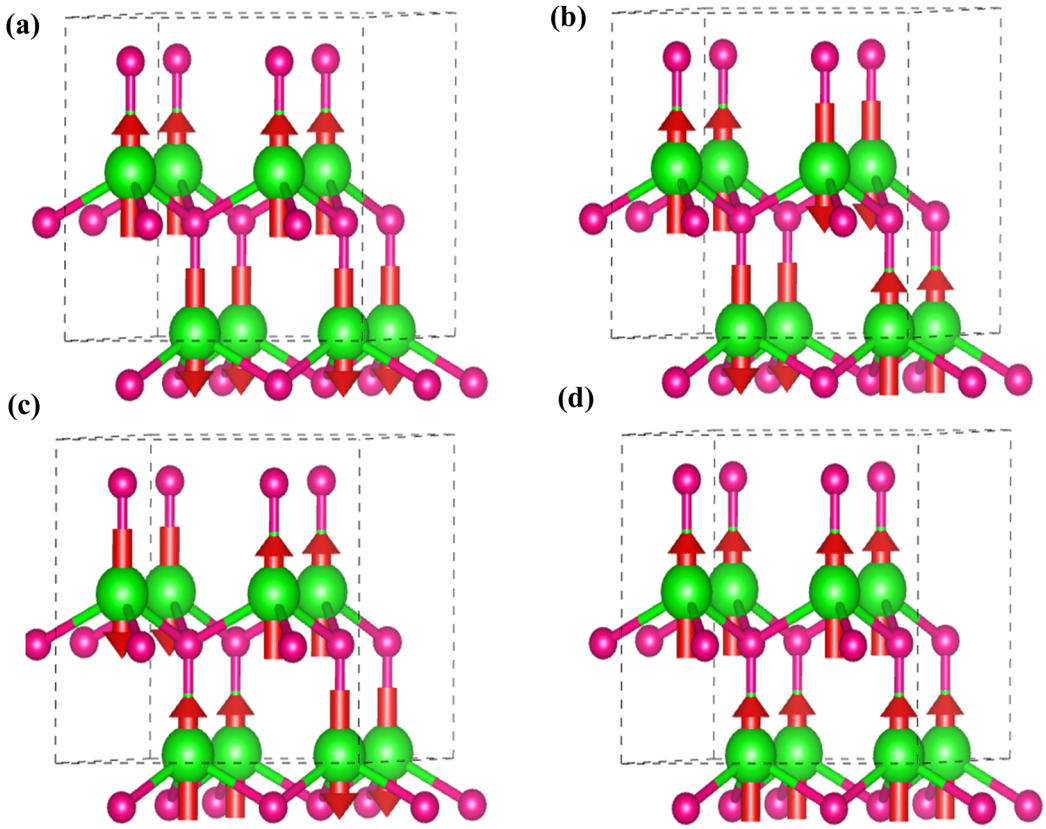

Fig. 2 Possible magnetic configurations of bulk wurtzite VO considered in this work (a) FM, (b) AFM1, (c) AFM2, and (d) AFM3. The figure shows representative ferromagnetic (FM) and antiferromagnetic (AFM) spin arrangements within a 2 × 2 × 1 supercell of the wurtzite structure. Green and pink spheres denote V and O atoms, respectively. Red arrows indicate the direction of the local magnetic moments on V atoms. These magnetic configurations were systematically compared to determine the magnetic ground state of w-VO.

prominent example is MoS_2, where the metallic 1T phase can be produced by chemical intercalation or exfoliation despite being ~0.8–0.9 eV per formula unit higher in energy than the semiconducting 2H ground state. Similar behavior has been reported for WS_2 and WSe_2, in which metastable 1T-like structures are accessible despite large energetic penalties.[36–41] These precedents demonstrate that polymorphs lying ~0.7–1.0 eV above the thermodynamic ground state can be stabilized through epitaxial constraint, charge transfer, or kinetic trapping. In this context, the wurtzite VO structure should be regarded as a metastable but physically meaningful configuration, suitable for exploring symmetry-driven electronic and magnetic phenomena, rather than as a thermodynamic ground state. The dynamical stability of w-VO was further verified through phonon dispersion analysis, as depicted in Fig. 3. The absence of any imaginary phonon frequencies throughout the entire Brillouin zone confirms that the crystal structure remains dynamically stable against small perturbations, substantiating its robustness under equilibrium conditions.[42]

The electronic band structure of the most stable antiferromagnetic (AFM) phase of bulk wurtzite VO, calculated without spin–orbit coupling (SOC), is shown in Fig. 4. The system exhibits a direct band gap of 0.68 eV at the Γ point. The spin-up (red) and spin-down (blue) bands overlap perfectly along the principal high-symmetry directions, indicating spin degeneracy at these specific k-points. This behavior is not accidental but is enforced by crystal symmetry. Bulk w-VO crystallizes in the non-

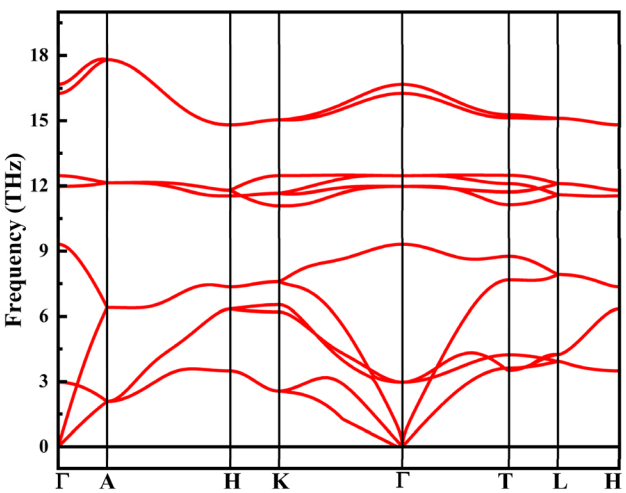

Fig. 3 Phonon dispersion relations of bulk wurtzite VO calculated along the high-symmetry directions of the hexagonal Brillouin zone. All phonon branches exhibit real (positive) frequencies throughout the Brillouin zone, indicating the dynamical stability of the optimized wurtzite VO structure.

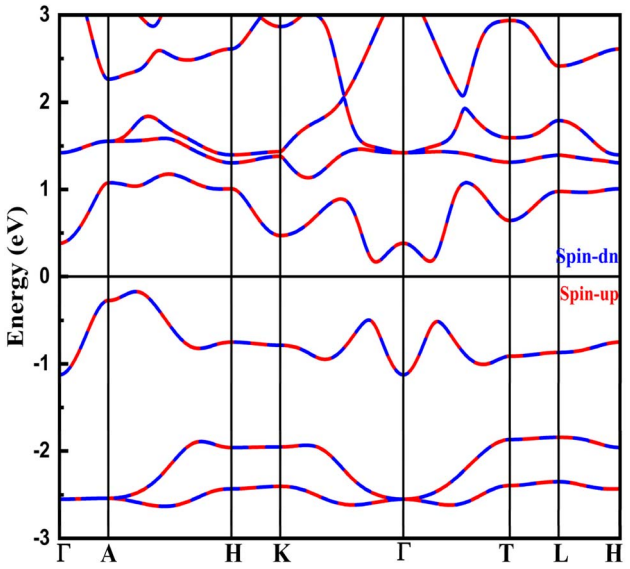

Fig. 4 Spin-resolved electronic band structure of bulk wurtzite VO calculated along the high-symmetry path of the hexagonal Brillouin zone. The red and blue curves denote the spin-up and spin-down channels, respectively. The Fermi level is set to 0 eV.

centrosymmetric hexagonal space group $P6_3mc$, which contains non-primitive symmetry operations that govern the spin degeneracy of the electronic states.

In particular, the magnetic structure preserves a twofold screw rotation symmetry, denoted as $\{C_{2z}|c/2\}$, which consists of a π rotation about the crystallographic *c*-axis followed by a translation of half a lattice vector along *c*. This symmetry operation maps one V sublattice onto the other while reversing the spin orientation, thereby relating opposite-spin electronic states at the same crystal momentum. As a result, spin degeneracy is protected along high-symmetry paths such as Γ–M–K–Γ–A–T–H–A, consistent with the band structure shown in Fig. 4. A schematic illustration of this symmetry mapping between the opposite-spin VO_4 tetrahedra is presented in Fig. 5(a). However, this symmetry protection does not extend to the entire Brillouin zone, because the two magnetic sublattices are not related by a pure lattice translation. Consequently, at generic (non-high-symmetry) *k*-points, the symmetry constraints are relaxed, allowing momentum-dependent spin splitting even in the absence of SOC. To demonstrate this effect, we computed the band structure along non-symmetric paths passing through the points (0.5, 0.0, 0.5), (0.0, 0.0, 0.0), and (0.0, 0.5, 0.5), as shown in Fig. 5(b). Clear spin splitting is observed in both the valence and conduction bands, with a maximum splitting of approximately 50 meV in the valence band. Despite the presence of this pronounced spin splitting, w-VO retains zero net magnetization due to its fully compensated AFM ground state. The coexistence of compensated magnetism with symmetry-allowed, momentum-dependent spin polarization identifies w-VO as an altermagnet, a distinct magnetic class in which spin polarization originates from crystal symmetry and magnetic order, rather than from relativistic spin–orbit interactions. Next, we analyzed the magneto-crystalline anisotropy energy (MAE) of bulk w-VO by performing non-collinear total energy calculations that explicitly included spin–orbit coupling (SOC). Our results indicate that the system exhibits an in-plane magnetic easy axis along the [100] direction, with a calculated MAE of 0.017 meV per unit cell (17 μeV per cell). To gain deeper insight into the spin-dependent transport behavior of bulk wurtzite VO, we analyzed its spin Hall conductivity (SHC), a quantity that

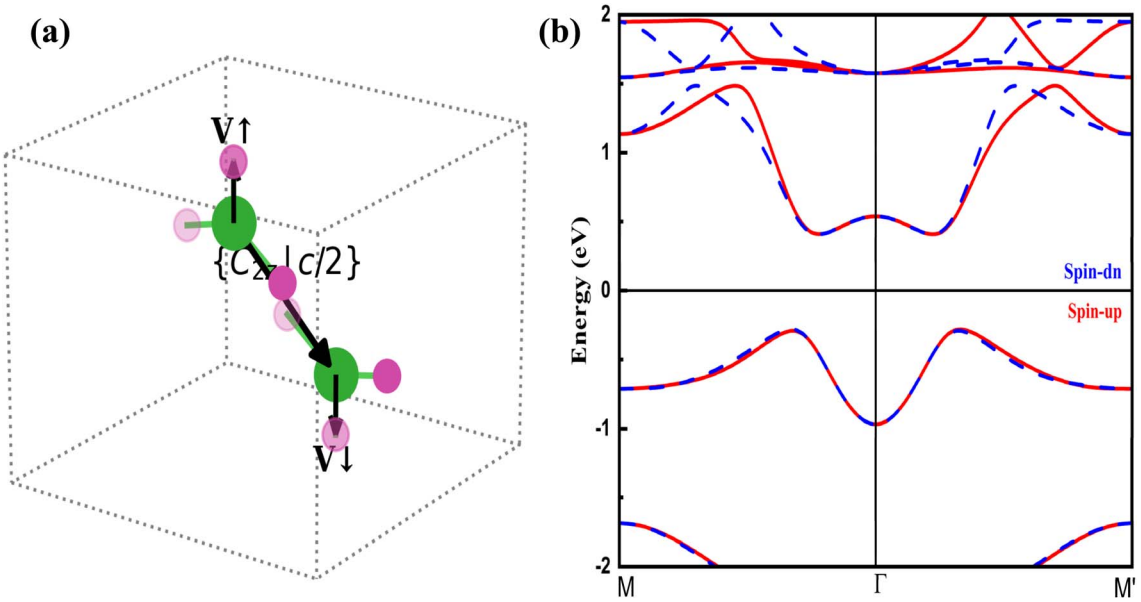

Fig. 5 (a) Two symmetry-related tetrahedra with opposite V spin orientations ($V_\uparrow$ and $V_\downarrow$) are connected by the non-primitive screw rotation $\{C_{2z}|c/2\}$, illustrating the symmetry origin of altermagnetism in wurtzite VO, and (b) spin-resolved electronic band structure of bulk wurtzite VO calculated along a non-symmetric *k*-path (M–Γ–M′). Red and blue curves denote the spin-up and spin-down channels, respectively. The non-symmetric path reveals a clear momentum-dependent spin splitting despite the compensated antiferromagnetic ground state.

characterizes the conversion of a longitudinal charge current into a transverse spin current due to spin–orbit coupling (SOC). Physically, when an electric field is applied along a given direction, SOC causes electrons with opposite spins to deflect in opposite transverse directions, producing a pure spin current even in the absence of magnetization.[43] The efficiency of this process is quantified by the SHC tensor $\sigma^{\mathrm{Spin}}_{\gamma\alpha\beta}$, where the indices α, β, and γ denote the directions of the electric field, charge current, and spin polarization, respectively. In this work, the spin Hall conductivity (SHC) of wurtzite VO was calculated including spin–orbit coupling (SOC) using the Kubo-Berry curvature formalism, which relates the SHC tensor components to the geometric properties of the electronic wave functions in momentum space. The Berry curvature acts as a magnetic field in reciprocal space, giving rise to an anomalous velocity that leads to the spin Hall effect. To achieve accurate integration over the Brillouin zone, the maximally localized Wannier functions (MLWFs) were constructed from the DFT-derived Bloch states, allowing precise interpolation of the band structure and Berry curvature on a dense k-point mesh.

Fig. 6 displays the calculated variation of SHC as a function of the chemical potential (μ) for the two tensor components $\sigma^{\mathrm{Spin}}_{xyz}$ and $\sigma^{\mathrm{Spin}}_{yzx}$, corresponding to spin polarization along the x and y directions, respectively. Owing to the semiconducting nature of w-VO with an energy gap of about 0.19 eV, both SHC components are nearly zero at the Fermi level, as there are no available carriers to contribute to spin transport in the intrinsic insulating state. However, as the Fermi level is shifted by doping, the situation changes markedly. Both components exhibit opposite signs at zero doping, implying that the spin currents generated along the two directions are of opposite orientation under the same electric field, an intrinsic feature arising from the anisotropic symmetry of the wurtzite lattice and the non-centrosymmetric distribution of the Berry curvature. Upon introducing charge carriers, we observe distinct trends in the two SHC components. The $\sigma^{\mathrm{Spin}}_{xzy}$ term remains relatively stable under both electron and hole doping, suggesting that the states contributing to this tensor component are weakly influenced by the Fermi level position. In contrast, the $\sigma^{\mathrm{Spin}}_{yzx}$ component exhibits a pronounced increase under hole doping, reaching a peak value of -182 $(\hbar/e)$ S cm^{-1} when μ is shifted to -0.39 eV. This strong response indicates that the valence band states near the Fermi level possess significant spin–orbit interaction and contribute effectively to transverse spin transport. The magnitude of SHC obtained here is considerably higher than those observed in several known spin Hall materials such as WTe_2 and V_2SeTeO monolayer altermagnets, which typically show values around 100 $(\hbar/e)$ S cm^{-1} or lower.[43,44] This enhanced SHC highlights the robust spin–orbit coupling and the unique symmetry of the wurtzite VO structure, both of which favor efficient spin current generation. Consequently, w-VO can be regarded as a promising candidate for spintronic applications, particularly in systems where coupling between ferroelectricity and spin transport could enable voltage-controlled spin Hall effects and multifunctional device architectures.

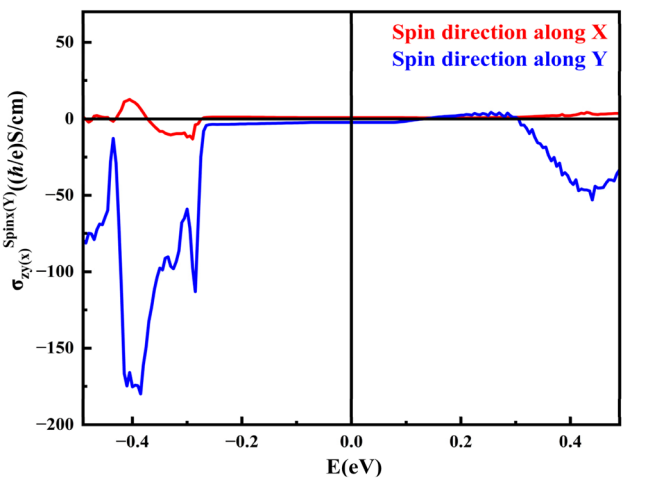

Fig. 6 Energy-dependent spin Hall conductivity of bulk wurtzite VO. The red and blue curves represent spin current polarized along the x and y directions, respectively. The vertical line at $E = 0$ eV denotes the Fermi level, highlighting the anisotropic spin Hall response near the Fermi energy.

Since bulk w-VO crystallizes in a polar space group that lacks mirror planes perpendicular to the c-axis, it is reasonable to anticipate a spontaneous out-of-plane electric polarization (P_s) along the [001] direction. To quantify P_s, we applied the modern theory of polarization, computing the difference between the polar and nonpolar phases of w-VO. The polarization is nonzero only along the [001] axis, with a calculated magnitude of 113.12 μC cm^{-2}, whereas it vanishes along the [100] and [010] directions. Because the Berry-phase polarization is defined modulo a polarization quantum, special care was taken to avoid branch ("wrapping") ambiguities. To this end, the polarization was evaluated along a continuous structural interpolation between the two symmetry-related polar states through a centrosymmetric reference configuration. The physically relevant polarization branch was selected by enforcing continuity of the polarization along the switching path, ensuring that no artificial jump by an integer multiple of the polarization quantum occurs. Upon gradually reducing the polarization from 113.12 μC cm^{-2} to zero, the system reaches a nonpolar state, and further displacement along the z-axis produces an opposite polarization of -113.12 μC cm^{-2}. The polarization evolution along this switching path is shown in Fig. 7(a) and (b), where the polarization varies continuously from +113.12 μC cm^{-2} to -113.12 μC cm^{-2} and smoothly crosses zero at the nonpolar configuration, confirming the absence of polarization-quantum wrapping and validating the extracted spontaneous polarization. The large spontaneous polarization arises primarily due to the significant electronegativity difference between V and O atoms. This P_s is notably higher than typical perovskites, such as $BaTiO_3$ (26 μC cm^{-2})[45] and Pb (Zr,Ti)O_3 (30–35 μC cm^{-2}),[46] and is comparable to ZnO (84–94 μC cm^{-2}).[19,47,48]

A defining feature of a ferroelectric material is switchable polarization under an applied electric field.[22] Although wurtzite-type ferroelectrics have historically been considered challenging to switch due to dielectric breakdown at high fields, we investigated a feasible switching pathway.[49] In our model, V

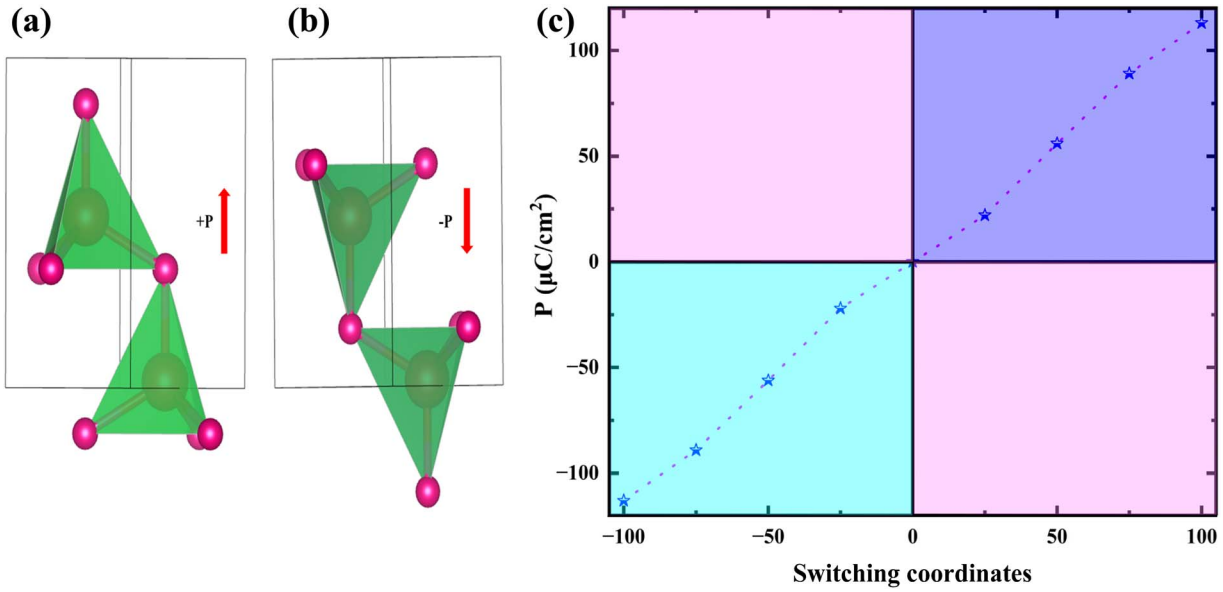

Fig. 7 (a) and (b) The switchable configurations for polarization of Wurtzite VO and (c) evolution of Berry-phase polarization (*P*) as a function of the switching coordinate λ for wurtzite VO. The polarization changes continuously from +113.12 μC cm^{-2} to −113.12 μC cm^{-2} and passes smoothly through zero at the nonpolar configuration, demonstrating a continuous polarization branch without polarization-quantum wrapping.

atoms were incrementally displaced downward along the *z*-axis relative to O atoms from the initial polar λ-phase, passing through a nonpolar intermediate state (λ)**, in which all V and O atoms lie in planes parallel to the basal ab-plane. From λ, V atoms were further displaced in steps of 0.04 Å until an opposite polarization state (−λ) was reached. The total displacement required to reverse the polarization was 0.34 Å.

The energy barrier for polarization switching represents the amount of energy required to reverse the direction of spontaneous polarization between two equivalent ferroelectric states. In this study, the nudged elastic band (NEB) method was employed to map the minimum energy pathway connecting these two polarization states in pristine wurtzite VO. As shown in Fig. 8, the calculated energy profile reveals a barrier height of 0.71 eV per formula unit, indicating that the two polarization states are separated by a finite but substantial energy barrier. While this barrier is larger than in conventional perovskite ferroelectrics, it is comparable to values reported for other wurtzite-derived polar materials.[50–52] Therefore, w-VO can be classified as an intrinsically ferroelectric system with robust spontaneous polarization, although practical polarization switching may require strong external fields, strain engineering, or reduced dimensionality. When we compared the electronic structures of the two opposite polarization states, we found a striking, reversible reorganization of the spin-resolved bands near the Fermi level. Fig. 9(a) and (b) displays the band structures computed for the polarization pointing "up" and for the polarization reversed ("down"). The reversed (negative) polarization retains the directional-dependent spin-splitting characteristic of an altermagnet, but several bands that carried majority-spin character in the positive-polarization state acquire the opposite spin character after switching. In other words, bands that were spin-up at certain *k*-points become spin-down (and *vice versa*) when the ferroelectric distortion is inverted. This behavior can be understood as a consequence of how ferroelectric displacements modify the local electronic environment and the spin-dependent potentials. Reversing the polarization flips the sign of the internal electric field and changes the pattern of atomic displacements, which alters crystal-field splitting and the effective hopping amplitudes between atoms. Because the spin splitting in an altermagnet is strongly tied to the lattice symmetry and to sublattice-

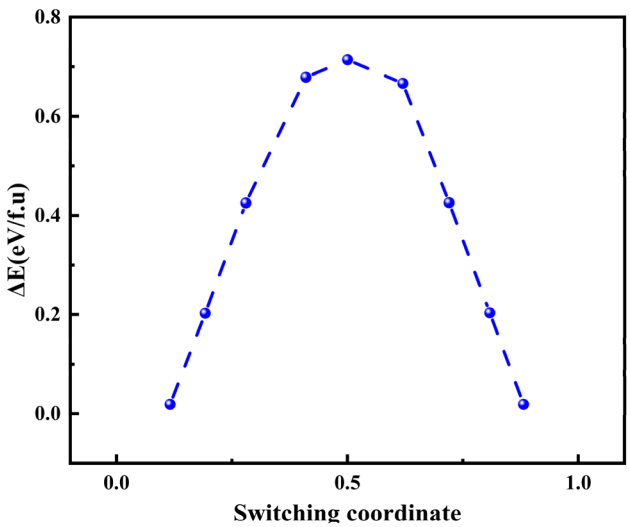

Fig. 8 Minimum energy pathway for polarization switching in bulk wurtzite VO obtained using the nudged elastic band (NEB) method. The energy profile shows two symmetry-equivalent polar states connected through a nonpolar saddle point, with a maximum barrier of ~0.71 eV per formula unit. This result demonstrates the energetic feasibility of polarization reversal in wurtzite VO.

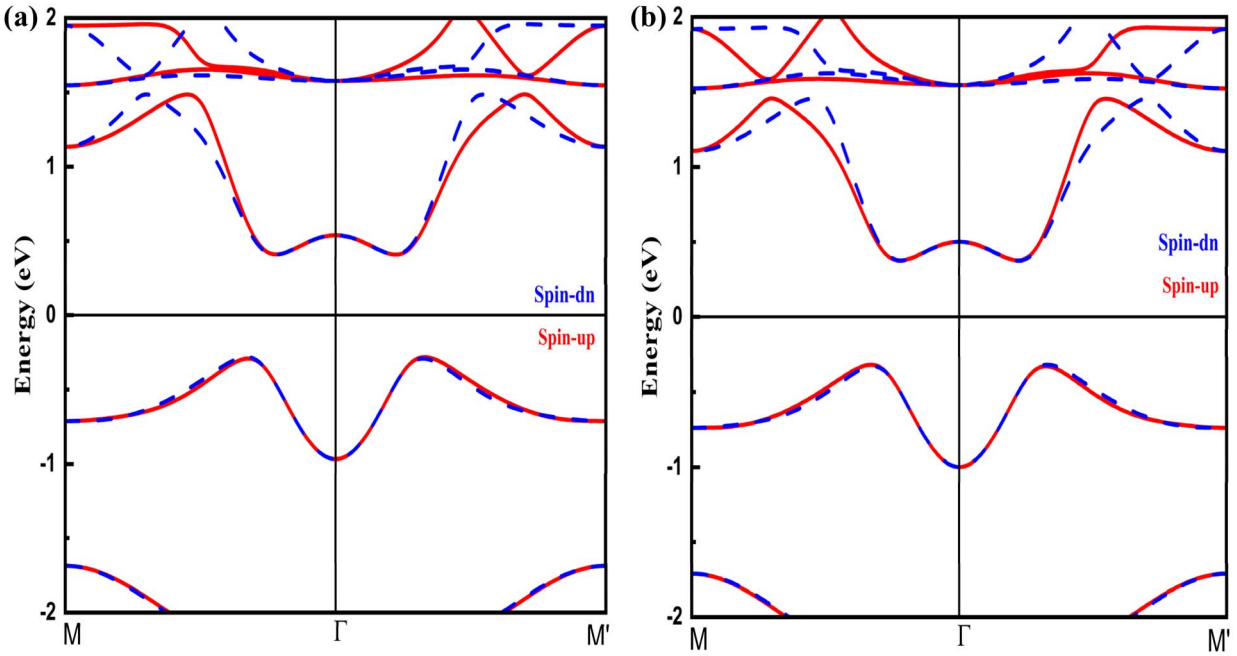

Fig. 9 Spin-resolved electronic band structure of bulk wurtzite VO calculated along the non-symmetric M–Γ–M′ path for two opposite polarization states: (a) positive polarization (+*P*) and (b) negative polarization (−*P*). Red and blue curves denote the spin-up and spin-down channels, respectively, with the Fermi level set to 0 eV. The reversal of polarization leads to a corresponding reversal of the momentum-dependent spin character, demonstrating polarization-controlled spin texture in wurtzite VO.

dependent exchange/SOC fields (rather than to a uniform macroscopic magnetization), changing those local potentials reverses the momentum-resolved spin splitting. The result is a band-selective exchange of spin character near the Fermi energy: the states that dominate transport or low-energy excitations change their spin polarization simply by flipping the ferroelectric order. The practical consequence is important: the spin polarization of carriers (and therefore spin-dependent responses such as spin currents, spin Hall signals, or spin-polarized conductivity) can be controlled electrically and non-volatile by switching the ferroelectric polarization. This does not necessarily create a large net magnetic moment (altermagnets usually have negligible net magnetization), but it does reverse which spin channel, at particular *k*-points and energy windows which dominates conduction. That provides a route to voltage-controlled spintronic functionality (for example, toggling the sign or magnitude of spin Hall or spin-Seebeck responses) without the need for magnetic fields. Overall, our results demonstrate that w-VO exhibits both robust ferroelectricity and altermagnetism, making it a rare example of a multifunctional material where switchable polarization coexists with spin-compensated magnetic order. This coexistence offers an exciting platform for exploring coupled ferroelectric, altermagnetic phenomena in both theoretical studies and experimental implementations.

Conclusion

In summary, first-principles calculations reveal that bulk wurtzite vanadium oxide (w-VO) is a dynamically and thermodynamically stable material that simultaneously hosts ferroelectric and altermagnetic order, establishing it as a new member of the multiferroic family. Structurally, w-VO adopts a non-centrosymmetric $P6_3mc$ wurtzite phase, where the layered antiferromagnetic configuration represents the ground state with zero net magnetization. The presence of alternating spin splitting of ∼50 meV in momentum space confirms its altermagnetic character, driven by crystal symmetry and magnetic sublattice exchange rather than spin–orbit coupling. Moreover, w-VO exhibits a large spontaneous polarization of 113.12 μC cm^{-2} along the [001] axis and a moderate energy barrier (0.71 eV per f.u.) for polarization reversal, signifying robust and switchable ferroelectricity. Importantly, polarization switching reverses the spin character near the Fermi level, thereby enabling electric-field control of spin-dependent electronic properties. The calculated spin Hall conductivity, reaching up to −182 $(\hbar/e)$S cm^{-1} under hole doping, highlights strong spin–orbit interactions and efficient spin-current generation. These results demonstrate that w-VO integrates ferroelectricity and altermagnetism in a single crystalline phase, enabling a direct coupling between electric polarization and spin transport. This coexistence provides a novel route toward designing multifunctional spintronic devices, where spin polarization, spin Hall response, and magnetic anisotropy can be tuned *via* ferroelectric control, offering an exciting platform for future electrically controllable, field-free spin-based technologies.

Conflicts of interest

The authors declare no conflict of interest.

Data availability

The data will be made available on a reasonable request.

Acknowledgements

The authors extend their appreciation to the Deanship of Research and Graduate Studies at King Khalid University, Kingdom of Saudi Arabia for funding this work through the Large Research Group Project under the grant number RGP.2/146/46.

References

1 M. S. Song, L. Houben, N. Rothem, A. Gupta, S. Rabkin, B. Kalisky and H. Beidenkopf, Shtrikman. Topotactic growth of Zintl phase Eu5In2As6 nanowires with antiferromagnetic behavior, *Nano Lett.*, 2025, **25**(18), 7292–7297.

2 S. Lee, S. Lee, S. Jung, J. Jung, D. Kim, Y. Lee, B. Seok, J. Kim, B. G. Park, L. Šmejkal and C. J. Kang, Broken Kramers degeneracy in altermagnetic MnTe, *Phys. Rev. Lett.*, 2024, **132**(3), 036702.

3 Y. Zhu, T. Chen, Y. Li, L. Qiao, X. Ma, C. Liu, T. Hu, H. Gao and W. Ren, Multipiezo effect in altermagnetic V2SeTeO monolayer, *Nano Lett.*, 2023, **24**(1), 472–478.

4 H. F. Chen, X. Y. Tao, B. H. Zhu, J. T. Pan, L. L. Ma, C. Chen, W. G. Zhu, W. Chen and Y. Q. Lu, Reconfigurable nonlinear Pancharatnam-Berry diffractive optics with photopatterned ferroelectric nematics, *Light: Sci. Appl.*, 2025, **14**(1), 314.

5 M. Lebedev and J. Akedo, Effect of thickness on the piezoelectric properties of lead zirconate titanate films fabricated by aerosol deposition method, *Jpn. J. Appl. Phys.*, 2002, **41**(11S), 6669.

6 Z. Feng, X. Zhou, L. Šmejkal, L. Wu, Z. Zhu, H. Guo, R. González-Hernández, X. Wang, H. Yan, P. Qin and X. Zhang, An anomalous Hall effect in altermagnetic ruthenium dioxide, *Nat. Electron.*, 2022, **5**(11), 735–743.

7 M. Leiviskä, J. Rial, A. Bad'ura, R. L. Seeger, I. Kounta, S. Beckert, D. Kriegner, I. Joumard, E. Schmoranzerová, J. Sinova and O. Gomonay, Anisotropy of the anomalous Hall effect in thin films of the altermagnet candidate Mn5Si3, *Phys. Rev. B*, 2024, **109**(22), 224430.

8 L. N. Oveshnikov, V. A. Kulbachinskii, A. B. Davydov, B. A. Aronzon, I. V. Rozhansky, N. S. Averkiev, K. I. Kugel and V. Tripathi, Berry phase mechanism of the anomalous Hall effect in a disordered two-dimensional magnetic semiconductor structure, *Sci. Rep.*, 2015, **5**(1), 17158.

9 R. J. Clément, Z. Lun and G. Ceder, Cation-disordered rocksalt transition metal oxides and oxyfluorides for high energy lithium-ion cathodes, *Energy Environ. Sci.*, 2020, **13**(2), 345–373.

10 L. Qiao and M. T. Swihart, Solution-phase synthesis of transition metal oxide nanocrystals: Morphologies, formulae, and mechanisms, *Adv. Colloid Interface Sci.*, 2017, **244**, 199–266.

11 M. A. Cambaz, B. P. Vinayan, H. Euchner, R. E. Johnsen, A. A. Guda, A. Mazilkin, Y. V. Rusalev, A. L. Trigub, A. Gross and M. Fichtner, Design of nickel-based cation-disordered rock-salt oxides: the effect of transition metal (M= V, Ti, Zr) substitution in LiNi0. 5M0. 5O2 binary systems, *ACS Appl. Mater. Interfaces*, 2018, **10**(26), 21957–21964.

12 K. M. Nam, Y. I. Kim, Y. Jo, S. M. Lee, B. G. Kim, R. Choi, S. I. Choi, H. Song and J. T. Park, New crystal structure: synthesis and characterization of hexagonal wurtzite MnO, *J. Am. Chem. Soc.*, 2012, **134**(20), 8392–8395.

13 S. Sawada, S. Hirotsu, H. Iwamura and Y. Shiroishi, A ferroelectric type of hysteresis loop observed in BeO, *J. Phys. Soc. Jpn.*, 1973, **35**(3), 946.

14 A. O. Onodera, N. T. Tamaki, Y. K. Kawamura, T. S. Sawada and H. Y. Yamashita, Dielectric activity and ferroelectricity in piezoelectric semiconductor Li-doped ZnO, *Jpn. J. Appl. Phys.*, 1996, **35**(9S), 5160.

15 M. Joseph, H. Tabata and T. Kawai, Ferroelectric behavior of Li-doped ZnO thin films on Si (100) by pulsed laser deposition, *Appl. Phys. Lett.*, 1999, **74**(17), 2534–2536.

16 P. Gopal, N. A. Spaldin and U. V. Waghmare, First-principles study of wurtzite-structure MnO, *Phys. Rev. B: Condens. Matter Mater. Phys.*, 2004, **70**(20), 205104.

17 A. Malashevich and D. Vanderbilt, First-principles study of polarization in Zn1−xMgxO, *Phys. Rev. B: Condens. Matter Mater. Phys.*, 2007, **75**(4), 045106.

18 C. A. Dal, M. Posternak, R. Resta and A. Baldereschi, Ab initio study of piezoelectricity and spontaneous polarization in ZnO, *Phys. Rev. B: Condens. Matter Mater. Phys.*, 1994, **50**(15), 10715.

19 H. Moriwake, R. Yokoi, A. Taguchi, T. Ogawa, C. A. Fisher, A. Kuwabara, Y. Sato, T. Shimizu, Y. Hamasaki, H. Takashima and M. Itoh, A computational search for wurtzite-structured ferroelectrics with low coercive voltages, *APL Mater.*, 2020, **8**(12), 121102.

20 S. Massidda, R. Resta, M. Posternak and A. Baldereschi, Polarization and dynamical charge of ZnO within different one-particle schemes, *Phys. Rev. B: Condens. Matter Mater. Phys.*, 1995, **52**(24), R16977.

21 F. Bernardini, V. Fiorentini and D. Vanderbilt, Spontaneous polarization and piezoelectric constants of III-V nitrides, *Phys. Rev. B:Condens. Matter Mater. Phys.*, 1997, **56**(16), R10024.

22 S. Fichtner, N. Wolff, F. Lofink, L. Kienle and B. Wagner, AlScN: A III-V semiconductor based ferroelectric, *J. Appl. Phys.*, 2019, **125**(11), 114103.

23 Y. Uetsuji, E. Nomura, K. Koike, S. Sasa, M. Inoue and M. Yano, First-Principles study on the spontaneous polarization of wurtzite Zm-xMgxO alloy crystals, *Zairyo*, 2009, **58**(3), 243–250.

24 F. Bernardini, V. Fiorentini and D. Vanderbilt, Accurate calculation of polarization-related quantities in semiconductors, *Phys. Rev. B: Condens. Matter Mater. Phys.*, 2001, **63**(19), 193201.

25 G. Y. Zhang, L. L. Ma, E. Lin, Z. Y. Wang, J. T. Pan, J. Yang, M. Deng, Y. Wei, Y. Ye, N. Wang and Y. Wang,

Periodically-modulated unipolar and bipolar orders in nematic fluids towards miniaturized nonlinear vectorial optics, *Nat. Commun.*, 2025, **16**(1), 9419.

26 G. Kresse and D. Joubert, From ultrasoft pseudopotentials to the projector augmented-wave method, *Phys. Rev. B: Condens. Matter Mater. Phys.*, 1999, **59**(3), 1758.

27 C. Yang, L. L. Yin, F. Bebensee, M. Buchholz, H. Sezen, S. Heissler, J. Chen, A. Nefedov, H. Idriss, X. Q. Gong and C. Wöll, Chemical activity of oxygen vacancies on ceria: a combined experimental and theoretical study on CeO2 (111), *Phys. Chem. Chem. Phys.*, 2014, **16**(44), 24165–24168.

28 W. Zhang, E. Zhu, Z. Li and H. Lv, Strain-tunable spin-valley locking and the influence of spin-orbit coupling in the two-dimensional altermagnet V2Te2O, *Phys. Rev. B*, 2025, **112**(14), 144427.

29 Q. Ma, B. Wang, G. Yang and Y. Liu, Multifunctional altermagnet with large out-of-plane piezoelectric response in Janus V2AsBrO monolayer, *Appl. Phys. Lett.*, 2025, **126**(22), 223106.

30 A. Zaman, K. Husain, S. H. Alrefaee, H. Shahid, M. Elhadi, A. Nurmuhammedov, R. M. Mohammed, V. Tirth, A. Algahtani and N. Elboughdiri, Multipiezo effect in altermagnet V2SeO monolayer at high temperature, *Case Stud. Therm. Eng.*, 2025, 106943.

31 Y. Zhu, T. Chen, Y. Li, L. Qiao, X. Ma, C. Liu, T. Hu, H. Gao and W. Ren, Multipiezo effect in altermagnetic V2SeTeO monolayer, *Nano Lett.*, 2023, **24**(1), 472–478.

32 J. P. Perdew, K. Burke and M. Ernzerhof, Generalized gradient approximation made simple, *Phys. Rev. Lett.*, 1996, **77**(18), 3865.

33 A. Togo, F. Oba and I. Tanaka, First-principles calculations of the ferroelastic transition between rutile-type and CaCl 2-type SiO2 at high pressures, *Phys. Rev. B: Condens. Matter Mater. Phys.*, 2008, **78**(13), 134106.

34 R. D. King-Smith and D. Vanderbilt, Theory of polarization of crystalline solids, *Phys. Rev. B*, 1993, **47**(3), 1651.

35 G. Henkelman, B. P. Uberuaga and H. Jónsson, A climbing image nudged elastic band method for finding saddle points and minimum energy paths, *J. Chem. Phys.*, 2000, **113**(22), 9901–9904.

36 B. A. Hanedar and M. C. Onbaşlı, Defect dependent electronic properties of two-dimensional transition metal dichalcogenides (2H, 1T, and 1T′ phases), *Phys. Chem. Chem. Phys.*, 2025, **27**(4), 1809–1818.

37 Z. Li, P. Sun, X. Zhan, Q. Zheng, T. Feng, P. V. Braun and S. Qi, Metallic 1T phase MoS2/MnO composites with improved cyclability for lithium-ion battery anodes, *J. Alloys Compd.*, 2019, **796**, 25–32.

38 J. Yi, X. She, Y. Song, M. Mao, K. Xia, Y. Xu, Z. Mo, J. Wu, H. Xu and H. Li, Solvothermal synthesis of metallic 1T-WS2: a supporting co-catalyst on carbon nitride nanosheets toward photocatalytic hydrogen evolution, *Chem. Eng. J.*, 2018, **335**, 282–289.

39 Z. J. Yang, Z. Li, G. I. Lampronti, J. I. Lee, Y. Wang, J. Day and M. Chhowalla, Environmental and thermal stability of chemically exfoliated li x mos2 for lithium–sulfur batteries, *Chem. Mater.*, 2024, **36**(9), 4829–4837.

40 M. S. Sokolikova, P. C. Sherrell, P. Palczynski, V. L. Bemmer and C. Mattevi, Direct solution-phase synthesis of 1T'WSe2 nanosheets, *Nat. Commun.*, 2019, **10**(1), 712.

41 A. Schrön, C. Rödl and F. Bechstedt, Energetic stability and magnetic properties of MnO in the rocksalt, wurtzite, and zinc-blende structures: Influence of exchange and correlation, *Phys. Rev. B: Condens. Matter Mater. Phys.*, 2010, **82**(16), 165109.

42 M. Sajjad, U. A. Khan, H. Ullah, A. Alhodaib, M. Amami, V. Tirth and A. Zaman, Structural, electronic, magnetic and elastic properties of xenon-based fluoroperovskites XeMF 3 (M= Ti, V, Zr, Nb) via DFT studies, *RSC Adv.*, 2022, **12**(42), 27508–27516.

43 J. Zhou, J. Qiao, A. Bournel and W. Zhao, Intrinsic spin Hall conductivity of the semimetals MoTe 2 and WTe 2, *Phys. Rev. B*, 2019, **99**(6), 060408.

44 J. Qiao, J. Zhou, Z. Yuan and W. Zhao, Calculation of intrinsic spin Hall conductivity by Wannier interpolation, *Phys. Rev. B*, 2018, **98**(21), 214402.

45 D. Damjanovic, Ferroelectric, dielectric and piezoelectric properties of ferroelectric thin films and ceramics, *Rep. Prog. Phys.*, 1998, **61**(9), 1267.

46 M. Lebedev and J. Akedo, Effect of thickness on the piezoelectric properties of lead zirconate titanate films fabricated by aerosol deposition method, *Jpn. J. Appl. Phys.*, 2002, **41**(11S), 6669.

47 E. Martínez-Aguilar, J. Ribas-Ariño and J. S. Beltrones, Structural, electronic and ferroelectric properties of Zn93.75M6.25O (M= Sr, Ba): first-principles calculations, *Scr. Mater.*, 2020, **187**, 8–12.

48 A. Konishi, T. Ogawa, C. A. Fisher, A. Kuwabara, T. Shimizu, S. Yasui, M. Itoh and H. Moriwake, Mechanism of polarization switching in wurtzite-structured zinc oxide thin films, *Appl. Phys. Lett.*, 2016, **109**(10), 102903.

49 H. Wang, N. Adamski, S. Mu and C. G. Van de Walle, Piezoelectric effect and polarization switching in Al1− x Sc x N, *J. Appl. Phys.*, 2021, **130**(10), 104101.

50 H. Moriwake, B. Akkopru-Akgun, S. Calderon, E. C. Dickey and P. Gorai, Physics of wurtzite ferroelectrics, *MRS Bull.*, 2025, **50**(9), 1066–1078.

51 C. W. Lee, N. U. Din, K. Yazawa, G. L. Brennecka, A. Zakutayev and P. Gorai, Emerging materials and design principles for wurtzite-type ferroelectrics, *Matter*, 2024, **7**(4), 1644–1659.

52 S. Song, H. M. Jang, N. S. Lee, J. Y. Son, R. Gupta, A. Garg, J. Ratanapreechachai and J. F. Scott, Ferroelectric polarization switching with a remarkably high activation energy in orthorhombic GaFeO3 thin films, *NPG Asia Mater.*, 2016, **8**(2), e242.